Infrared emittance of Ni_x–Cr_{1-x} alloys

2004 J. Phys.: Condens. Matter 16 2129

(http://iopscience.iop.org/0953-8984/16/12/022)

INSTITUTE OF PHYSICS PUBLISHING JOURNAL OF PHYSICS: CONDENSED MATTER

J. Phys.: Condens. Matter **16** (2004) 2129–2138 PII: S0953-8984(04)73762-5

Infrared emittance of Ni_x–Cr_{1-x} alloys

K Gelin[1] **and E Wäckelgård**

Division of Solid State Physics, Department of Engineering Sciences, Uppsala University, Box 534, SE-751 21 Uppsala, Sweden

E-mail: Kristina.Gelin@angstrom.uu.se

Received 19 December 2003
Published 12 March 2004
Online at stacks.iop.org/JPhysCM/16/2129 (DOI: 10.1088/0953-8984/16/12/022)

Abstract

The purpose of this study was to investigate the relation between the infrared emittance (at 10 μm) and the alloy concentration for Ni_xCr_{1-x} and to find out if the Hagen–Ruben relation could be applicable to this system. The work showed that the Hagen–Ruben relation was valid for the nickel-rich fcc-phase alloys from 11–43% Cr. This indicates that intraband transitions dominate over interband transitions in the infrared wavelength range due to impurity scattering. It was also found that an integrated formulation of the Hagen–Ruben relation could be used for the integrated room temperature thermal emittance. A similar study has recently been performed on the Cu_yNi_{1-y} fcc-phase system where the Hagen–Ruben relation was valid for both copper-rich and nickel-rich alloys.

1. Introduction

The motivation of this work was to study the infrared emittance of Ni–Cr alloys. Infrared emittance of metals is of interest in thermal radiant applications such as heat mirrors and spectrally selective solar absorbers.

The nickel–chromium system forms a solid solution over a rather wide range of concentrations [1], over 60% at eutectic (1070 K). The nickel-rich alloy has an fcc atomic arrangement and the chromium-rich phase has a bcc arrangement. Chromium increases the lattice spacing of nickel and nickel decreases the spacing of chromium [2]. From about 45% to 85% Cr the nickel-rich fcc phase and the chromium-rich bcc phase co-exist. An inter-metallic compound, Ni_2Cr, can be formed from annealing, but on rapid cooling of the melt the structure becomes disordered [1]. Atomic clustering can also be promoted by annealing [3]. At room temperature the alloys are paramagnetic with more than about 6% of chromium. Nickel–chromium alloys are used in many technical applications due to their corrosion resistance. Alloys containing 13–20% chromium are then mostly used.

Resistivity data usually exist or can easily be measured for all types of metals. It is therefore of interest to investigate if the infrared emittance, which requires more sophisticated

[1] Author to whom any correspondence should be addressed.

measurements, could be estimated from resistivity measurements by using such a simple relation between resistivity and infrared reflectance as the Hagen–Ruben relation. A similar study had earlier been performed on the copper–nickel alloy over the whole concentration range [4]. The conclusions from that study were that the Hagen–Rubens relation could be verified for both the copper- and nickel-rich alloys. It was therefore assumed that strong electron scattering from impurities made intraband transitions dominate over interband transitions in the infrared wavelength range. The validity of the Hagen–Rubens relation could, as a good approximation, be used for the integrated thermal emittance in the copper- and nickel-rich cases.

Nickel and chromium, both 3d-transition metals, have a large difference in the number of electrons in unfilled shells (chromium has six and nickel has nine) but a very small mass difference. These properties have made NiCr interesting from a theoretical point of view to study as a representative of a disordered system with large orbital differences and a small mass disorder. Electron band-structure calculations [5] for fcc NiCr alloys, using the coherent potential approximation (CPA), show that virtual bound states (VBS) appear at low chromium concentrations in the vicinity of the alloy Fermi level, making the density of state at the Fermi level much higher for both the majority and minority spin states compared to pure nickel. The CPA approach is supported by experimental studies of transport and magnetic properties [5]. As the chromium concentration increases the density of states at the Fermi levels remains high and the partial density of state of Cr has a peak at the Fermi level in the whole concentration range for the nickel-rich fcc phase. The optical properties of nickel and chromium cannot be described by the Drude theory since d-band states in the vicinity of the Fermi level make interband optical transitions dominate the optical absorption in the infrared region [6]. Hence the Hagen–Rubens relation is not valid for pure nickel or chromium in the near-infrared wavelength range around 10 μm. The situation for disordered NiCr could be the opposite, i.e. intraband absorption could dominate if impurity scattering is strong.

The optical properties of NiCr had earlier been studied for the nickel-rich alloys in the wavelength range 0.25–17 μm and alloy concentrations from 2 to 32% Cr [7–9]. The optical absorption was studied in terms of the optical conductivity and discussed in terms of electronic interband transitions in pure nickel. The inter- and intraband optical conductivity were separated in intraband and interband processes using a two-band model for the interband contribution. According to [8] the Hagen–Rubens relation fits to experimental data in the wavelength range 12–17 μm.

If intraband absorption dominates due to strong impurity scattering we would expect the emittance to change with composition in a similar manner as the dc electrical resistivity according to the Hagen–Rubens relation. In disordered alloys, the dc electrical resistivity shows a gradual increase with increased concentration of one of the constituents in the alloy and it reaches a maximum value at about equal concentrations of both. The resistivity can be described by the Nordheim rule for noble metals with similar atomic volumes and the same valence and crystal structures [10].

In the following study the emittance was derived from reflectance measurements on NiCr samples covering the whole compositional range. The purpose was to establish a relation between the alloy concentration and infrared emittance for wavelengths of the order of 10 μm, which is of interest in room temperature radiant applications.

2. Theoretical framework

The Hagen–Rubens relation is usually expressed as the spectral reflectance $R(\omega)$ at normal angle of incidence as a function of the frequency ω [10]:

$$R(\omega) = 1 - 2\left[\frac{2\varepsilon_0\omega}{\sigma_0}\right]^{1/2} \tag{1}$$

where σ_0 is the dc electrical conductivity and ε_0 is the vacuum permittivity. The dc electrical conductivity for metal, according to the Drude model, depends on the free electron concentration n_e, the relaxation time τ and the effective electron mass m^* [11]:

$$\sigma_0 = \frac{n_e e^2 \tau}{m^*}. \tag{2}$$

It is then assumed that the relaxation time is frequency-independent which is the case if scattering from neutral impurities is the dominating relaxation process [12]. Substituting reflectance for emittance ε (valid for bulk metals) and the electrical conductivity with the inverse of the electrical resistivity ρ, equation (1) can be expressed as the emittance as a function of wavelength λ ($\lambda = 2\pi c/\omega$, where c is the light velocity in vacuum):

$$\varepsilon(\lambda) = 2\left[\frac{4\pi\varepsilon_0 c\rho_0}{\lambda}\right]^{1/2}. \tag{3}$$

The near-normal thermal emittance, ε_t, was calculated as the average emittance weighted with the blackbody radiance distribution $I_b(\lambda, T)$ over the measured wavelength range, λ_1 to λ_2, in this case for T equal to room temperature (293 K):

$$\varepsilon_t = \frac{\int_{\lambda_1}^{\lambda_2} (1 - R(\lambda)) I_b(\lambda, T)\,\mathrm{d}\lambda}{\int_{\lambda_1}^{\lambda_2} I_b(\lambda, T)\,\mathrm{d}\lambda}. \tag{4}$$

The Hagen–Rubens relation is not strictly valid for the integrated emittance. In order to check if we can extend the validity of the Hagen–Rubens relation to the integrated emittance the same type of integration as in equation (4) was also performed on the right-hand side of equation (3), which from a mathematical point of view is formally correct. The constant factor in this integrated version of the Hagen–Rubens relation then includes the integration of $\lambda^{-1/2}$ weighted by the blackbody radiation distribution:

$$\varepsilon_t = \frac{\int_{\lambda_1}^{\lambda_2} 2\,[4\pi\varepsilon_0 c\rho_0/\lambda]^{1/2} I_b(\lambda, T)\,\mathrm{d}\lambda}{\int_{\lambda_1}^{\lambda_2} I_b(\lambda, T)\,\mathrm{d}\lambda}. \tag{5}$$

3. Sample preparation

Nine different bulk nickel–chromium alloys, a nickel and a chromium sample were manufactured by GfE Metalle und Materialen GmbH, Germany. The element content of the samples is shown in table 1. The nickel sample has a purity of 99.9% and the chromium sample 99.94%. The purities of the elements in the alloy samples are 99.8% for nickel and 99.8% for chromium. The samples were ordered in weight per cent and the manufacturer reported the tolerance of the alloy ratios with an uncertainty of ±2 wt%. According to the manufacturer the alloys were melted in a vacuum arc furnace and then water-cooled. All alloys were melted in the forms of ingots before they were cut out.

The samples were studied with x-ray diffraction in order to look at the present phases of the samples. The samples Ni, $Ni_{57}Cr_{43}$, $Ni_{67}Cr_{33}$, $Ni_{78}Cr_{22}$ and $Ni_{89}Cr_{11}$ consisted of a solid solution, disordered, nickel fcc phase. The samples $Ni_{18}Cr_{82}$, $Ni_{28}Cr_{72}$, $Ni_{37}Cr_{63}$ and $Ni_{47}Cr_{53}$ consisted of a mixture of crystallites of nickel-rich fcc phase and chromium-rich bcc phase. Ni_9Cr_{91} was in a disordered solid solution of chromium bcc phase. Table 1 contains the element content in atomic per cent together with the present phases of the alloys.

Table 1. The element content and phases of the manufactured nickel–chromium alloys.

Ni (at.%)	Cr (at.%)	Present phases
100	0	Fcc
89	11	Fcc
78	22	Fcc
67	33	Fcc
57	43	Fcc
47	53	Mix
37	63	Mix
28	72	Mix
18	82	Mix
9	91	Bcc
0	100	Bcc

The samples were prepared according to the same procedure as previously described for copper–nickel alloys [4]. All bulk samples were polished to obtain a smooth surface. Rods of a typical size 20 mm $\times$ 0.6 mm $\times$ 0.3 mm were cut from the bulk materials for the resistivity measurements. Samples for resistivity measurements were prepared from all samples except $Ni_{89}Cr_{11}$ since it was too brittle to be cut into such small samples.

4. Experimental measurements

The experimental set-up and procedure were identical with those in the study on copper–nickel alloys [4] and we have therefore chosen to only outline the main features of the experimental procedures.

4.1. Reflectance measurements

The near-normal specular reflectance, from 2 to 40 μm, was measured with a Perkin-Elmer 983 double beam spectrophotometer. Evaporated gold mirrors were used as references. The accuracy of the measurements, regarding systematic errors, was less than 0.01.

4.2. Resistivity measurements

A standard four-probe method was used in the resistance measurements. The voltage was recorded in the temperature range 77–293 K with a Hewlett Packard 3457A Multimeter instrument. The resistance of a platinum wire was used as a thermometer in the measurements. The sample thickness and width were measured with an accuracy of 0.02 mm and the distance between the two wires with an accuracy of 0.3 mm. A maximum error analysis was performed for each sample.

5. Results and discussion

5.1. Resistance measurements

The resistivity, ρ, of the nickel–chromium alloys at 293 K can be seen in figure 1. The resistivity of the alloys increases with chromium content up to $Ni_{57}Cr_{43}$, which comprises the data of the nickel-rich fcc phase in the paramagnetic phase. A four-degree polynomial is, as a guide to the eye, fitted to these data. The same polynomial is also indicated as a broken curve for the chromium-rich bcc phase. As mentioned earlier the Ni_9Cr_{91} sample could not be prepared

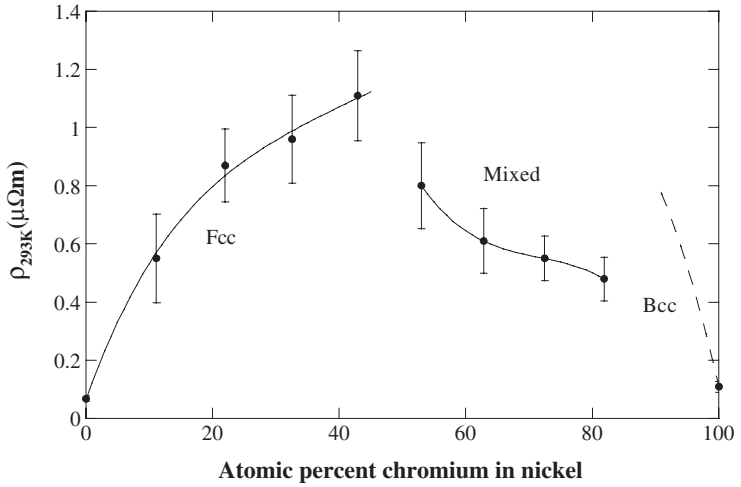

Figure 1. Resistivity at 293 K of nickel–chromium alloys. The maximum error is marked with error bars.

due to its brittleness, and resistivity data are therefore missing in the bcc phase. The resistivity of the mixed phase intermediate range shows a slight decrease in resistivity with increasing chromium content. A three-degree polynomial is, as a guide to the eye, connected to these data. The maximum error for each sample is marked in figure 1.

The resistivity of $Ni_{89}Cr_{11}$ and $Ni_{78}Cr_{22}$ are about 20% lower than previously published data up to 27% Cr [13]. The discrepancies might be due to metallurgical differences [3].

5.2. Reflectance measurements

The room temperature reflectance of the nickel-rich Ni–Cr alloys is shown in figure 2(a) and the chromium-rich in figure 2(b). The general appearance of both the nickel- and chromium-rich alloys is similar with a fairly constant reflectance for wavelengths longer than 20 μm. In contrast, the reflectance of pure nickel shows a rather high, fairly constant, reflectance from 10 to 40 μm. The interpretation is that interband transitions increase the absorption in the near-infrared wavelength range in the alloys as reported previously [14]. This is also expected from a theoretical point of view since chromium increases the density of states at the Fermi level due to the formation of a VBS which is responsible for an increase in low energy interband transitions. Hence a small addition of chromium changes the infrared reflectance so that the wavelength dependence becomes more like that of chromium than nickel. However the reflectance level is lower than for pure chromium.

The near-normal emittance at 10.5 μm was derived from the near-normal reflectance data in figures 2(a) and (b) as $\varepsilon(10.5\ \mu\text{m}) = 1 - R(10.5\ \mu\text{m})$. The wavelength of 10.5 μm was chosen since it is the wavelength of maximum intensity for the blackbody radiation at 293 K (radiation maximum for room temperature). In order to limit the influence of noise in the measured data, the reflectance at 10.5 μm was derived from a linear fit between 10.2 and 10.8 μm. The standard deviation was calculated to 0.001 and marked with error bars in figure 3(a). The emittance data points for the nickel-rich fcc and chromium-rich bcc phase are, as a guide to the eye, fitted to a four-degree polynomial as can be seen in figure 3(a). The emittance in the mixed phase intermediate region shows a step-like decrease of the emittance from 43% Cr to 53% Cr. The emittance decreases from 53% Cr to a minimum at 63% Cr and

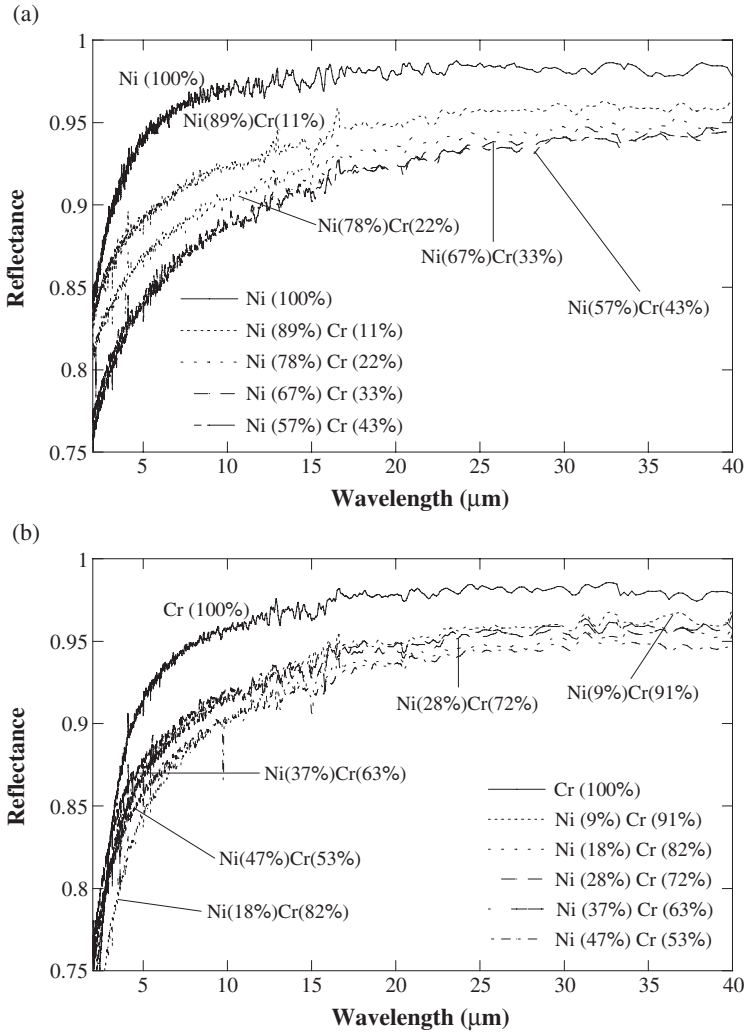

Figure 2. (a) Reflectance of nickel-rich nickel–chromium alloys. (b) Reflectance of chromium-rich nickel–chromium alloys.

then increases to 82% Cr. A more gradual decrease in the emittance in this mixed phase was expected as observed in the resistivity data in figure 1.

The integrated emittance as defined in equation (4) is often of more practical use when evaluating thermal radiant properties of surfaces. We have therefore calculated the integrated emittance from equation (4) at 293 K for all samples, which is shown in figure 3(b). The integrated emittance shows a similar dependence on alloy composition as the emittance at 10.5 μm.

5.3. Relation between the emittance and the resistance

Both the emittance at 10.5 μm and the integrated emittance for 293 K have a similar dependence on alloy composition as the resistivity and in order to check the validity of the Hagen–Rubens

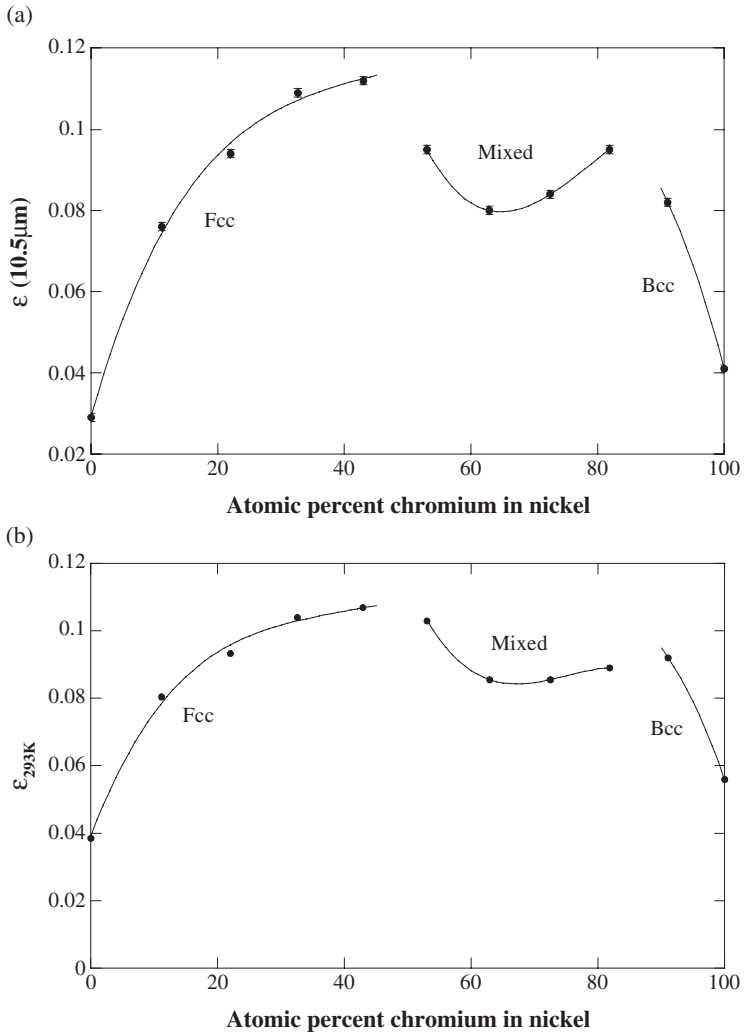

Figure 3. (a) Optical emittance, at 10.5 μm, of chromium–nickel alloys. The standard deviation is marked as error bars. (b) Thermal emittance, calculated at 293 K, of nickel–chromium alloys.

relation in equation (3) the emittance at 10.5 μm of the nickel-rich alloys was plotted versus the square root of the dc resistivity in figure 4(a). A line fit gives the slope 0.12 $\mu\Omega^{-1/2}$ $m^{-1/2}$. The standard deviation and the maximum error are marked for the emittance values and for the resistivity measurement with error bars in figure 4(a). Notice that the pure samples of nickel and chromium are excluded from the fit since they do not fulfil the conditions for the Hagen–Rubens relation since interband transitions dominate in the infrared wavelength range (see the introduction section).

The slope of the line is compared to the coefficient in the Hagen–Rubens relation in equation (3): $2(2\varepsilon_0\omega)^{1/2}$, which is 0.11 $\mu\Omega^{-1/2}$ $m^{-1/2}$ at 10.5 μm. Hence the agreement is good between experimental and theoretical values of the coefficient and it indicates that intraband transitions dominate the infrared optical properties in the nickel-rich fcc phase. Although the interband absorption is also strong due to the VBS at the Fermi level the disorder

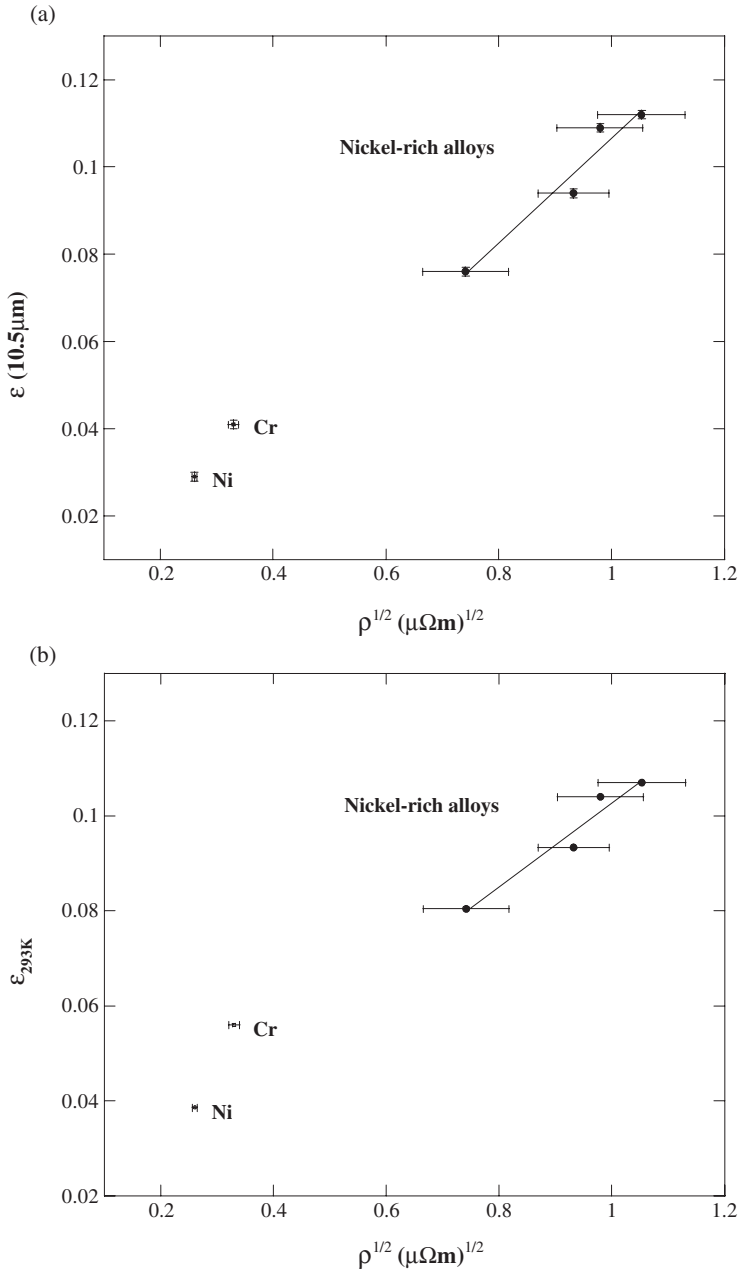

Figure 4. (a) Emittance at 10.5 μm versus the square root of resisitivity at 293 K, of nickel-rich alloys, nickel and chromium. A linear curve fit is included for the alloys. The horizontal error bars show the maximum error for the square root of the resistivity and the vertical error bars show the standard deviation for the optical emittance. (b) Thermal emittance versus the square root of resistivity, at 293 K, of nickel-rich alloys, nickel and chromium. A linear curve fit is included for the alloys. The error bars mark the maximum error for the square root of the resistivity.

causes strong impurity scattering. It has been assumed here using the simple Hagen–Rubens relation that the relaxation time is frequency-independent, which is valid for neutral impurities

according to previous studies [15]. Charge transfer between nickel and chromium is expected. The intersection of the linear curve with the ε axis in the diagram in figure 4(a) occurs at $\varepsilon = -0.01$, not at zero emittance as expected from equation (3). This means that the thermal emittance is lower, or the square root of the resistivity is larger, than expected from the Hagen–Rubens relation.

If the point zero emittance at zero resistivity is included in the fit the slope becomes 0.10 $\mu\Omega^{-1/2}$ $m^{-1/2}$. The calculated value of 0.11 $\mu\Omega^{-1/2}$ $m^{-1/2}$ from equation (3), and 0.10 $\mu\Omega^{-1/2}$ $m^{-1/2}$ when including the zero emittance, are both within the experimental errors.

The mixed phase alloys cannot be fitted to the Hagen–Rubens relation. We have, at the moment, no explanation for the difference between optical and dc electrical properties but grain sizes and borders might play a role. The dc resistance involves both intergrain and intragrain resistance while the emittance is only sensitive to intragrain responses from the electromagnetic field [16]. Since grain size distributions have not been determined this is only a speculation.

The integrated emittance values of the nickel-rich fcc-phase alloys have been plotted versus the square root of the resistivity in figure 4(b). A linear curve is fitted for the nickel-rich alloys giving a slope of 0.09 $\mu\Omega^{-1/2}$ $m^{-1/2}$. The maximum error is marked as error bars for the square root of the resisitivity in figure 4(b). The values for pure nickel and chromium are also excluded from the fit in this case.

The coefficient in the Hagen–Rubens relation should, in the case of integrated emittance, also be integrated over the same wavelength range as in equation (5). The coefficient at 293 K is 0.10 $\mu\Omega^{-1/2}$ $m^{-1/2}$ and the experimental values for the integrated emittance are slightly lower but within the experimental errors. This indicates that the integrated thermal emittance can be derived from measurement of the dc resistivity at room temperature for paramagnetic nickel-rich fcc-phase alloys. The intersection of the linear curve with the ε axis in the diagram of figure 4(b) occurs at $\varepsilon = 0.03$. As the integration is performed from 2.5 μm it includes a part of the experimental range where interband transitions contribute significantly to the spectral emittance. According to Gorban and Stashchuk [9], the spectral optical conductivity shows a dispersion related to interband transitions at least up to 5 μm. The interband contribution increases the integrated emittance but not the dc resistivity.

6. Conclusions

The infrared reflectance and dc resistivity were measured at room temperature for NiCr alloys over the whole concentration range. The Hagen–Rubens relation could be established for the nickel-rich paramagnetic fcc state in the concentration range 11–43% Cr. Hence it is concluded that high impurity levels are sufficiently high for intraband transitions to dominate from wavelengths longer than 10 μm.

The Hagen–Rubens relation could also be extended to the integrated thermal emittance at 293 K for the same group of samples (nickel-rich fcc-phase paramagnetic state in the concentration range 11–43% Cr) using an integrated coefficient in the relation and a constant addition of 0.03 in emittance correcting for interband contributions in the short wavelength range of the blackbody radiation.

We have so far investigated two different types of alloys: the copper–nickel alloy reported in [4] and the nickel–chromium alloy reported here. The CuNi alloy represents a system with small differences in the number of valence electrons and mass and the NiCr alloy represents a system with a large difference in the number of valence electron states and a small mass difference. For both these systems the thermal emittance and dc resistivity can be described by the Hagen–Rubens relation in the solid soluble fcc phase which, in the case of CuNi, extends

through the whole concentration range and for Cr concentrations less than 45% for NiCr. It would be interesting to study a larger group of alloys in order to investigate if resistivity and emittance correlate according to the simple Hagen–Rubens relation more generally or if there are some systems in which impurity scattering become less strong and interband transitions dominate.

Acknowledgments

A number of people have been supportive during the progress of this work. Among others the authors would like to mention Marie Wennström, Jesper Edert, Anders Hoel and Arne Roos. This project was financially supported by the Bengt Ingeström Foundation and the Swedish National Energy Administration.

References

[1] Smith J F, Carlson O N and Nash P G 1986 *Binary Alloy Phase Diagrams* vol 2 (Metals Park, OH: ASM International)
[2] Pearson W B 1958 *A Handbook of Lattice Spacings and Structures of Metals and Alloys* (London: Pergamon)
[3] Rana A M, Khan A F, Abbas A and Ansari M I 2003 *Mater. Chem. Phys.* **80** 228
[4] Gelin K and Wäckelgård E 2004 *J. Phys.: Condens. Matter* **16** 833
[5] Chakravarthy R and Madhav Rao L 1984 *J. Magn. Magn. Mater.* **43** 177
[6] Lenham A P 1967 *J. Opt. Soc. Am.* **57** 473
[7] Gorban N Ya, Stashchuk V S, Petrenko P V and Shishlovskii A A 1973 *Opt. Spectrosc.* **35** 400
[8] Gorban N Ya, Stashchuk V S and Shishlovskii A A 1974 *J. Appl. Spectrosc.* **20** 881
[9] Gorban N Ya and Stashchuk V S 1976 *Opt. Spectrosc.* **41** 291
[10] Mott N F and Jones H 1958 *The Theory of the Properties of Metals and Alloys* (New York: Dover)
[11] Kittel C 1996 *Introduction to Solid State Physics* 7th edn (New York: Wiley)
[12] Grosse P 1979 *Freie Elektronen in Festkörpern* (Berlin: Springer)
[13] Yao Y D, Arajs S and Anderson E E 1975 *J. Low Temp. Phys.* **31** 369
[14] Seib D H and Spicer W E 1970 *Phys. Rev.* B **2** 1676
[15] Staunton J B, Johnson D D and Pinski F J 1994 *Phys. Rev.* B **50** 1450
[16] Kim K H, Gu J Y, Choi H S, Eom D J, Jung J H and Noh T W 1997 *Phys. Rev.* B **55** 4023